Application of realistic effective interactions to the structure of the Zr isotopes

A. Holt, T. Engeland, M. Hjorth-Jensen, and E. Osnes
Department of Physics, University of Oslo, N-0316 Oslo, Norway
(Received 24 August 1999; published 19 May 2000)

We calculate the low-lying spectra of the zirconium isotopes ($Z=40$) with neutron numbers from $N=52$ to $N=60$ using the $1p_{1/2}0g_{9/2}$ proton and $2s1d0g_{7/2}0h_{11/2}$ neutron subshells to define the model space. Effective proton-proton, neutron-neutron, and proton-neutron interactions have been derived using ^{88}Sr as closed core and employing perturbative many-body techniques. The starting point is the nucleon-nucleon potential derived from modern meson exchange models. The comprehensive shell-model calculation performed in this work provides a qualitative reproduction of essential properties such as the subshell closures in ^{96}Zr and ^{98}Zr.

PACS number(s): 21.60.Cs, 27.60.+j

I. INTRODUCTION

The Zr isotopes undergo a clear and smooth shape transition with increasing neutron number. The isotopes which are displayed in Fig. 1(a) span from pure spherical nuclei that can be described in terms of simple shell-model configurations to the strongly deformed nucleus ^{102}Zr. Evidence for coexisting shapes has been reported around ^{100}Zr [1–4]. In the intermediate region, both ^{96}Zr and ^{98}Zr present evidence for subshell closure. These isotopes have a remarkably large gap between the ground state and the 2_1^+ level, 1.751 MeV in ^{96}Zr and 1.223 MeV in ^{98}Zr. They also have a relatively low level density below 3 MeV. Empirically, the Zr isotopes are fairly well established. Lhersonneau and collaborators have recently performed careful experimental studies of the Zr isotopes and neighboring nuclei, and they have made major contributions to the identification of levels in ^{97}Zr and ^{99}Zr [5].

For comparison the empirical Sr spectra are sketched in Fig. 1(b). The Sr isotopes differ from the Zr isotopes by only two protons but are qualitatively quite different. Compared to Zr the Sr isotopes have a much smoother behavior with a stable 0^+-2^+ spacing similar to that observed in tin. Large gaps due to subshell closure as observed in ^{96}Zr and ^{98}Zr do not occur in Sr. However, as in Zr there is a clear transition from spherical to deformed shape around $N=60$. The low-lying spectrum of ^{100}Sr is a nearly perfect rotational band. It is a theoretical challenge to describe a sequence of isotopes with such big changes in the structure from one nucleus to another as in Zr. For a proper description of the Zr isotopes one has to allow for proton excitations. In particular, the protons seem to play a dominant role in the 0_2^+ state. Thus, the common choice of inert core has been ^{88}Sr, though with large variations in the size of model space, truncation scheme and effective interactions, Refs. [6–8]. The early calculation by Auerbach and Talmi [9] was carried out with valence protons filling the $(1p_{1/2},0g_{9/2})$ oribitals and valence neutrons filling the $(1d_{5/2})$ orbital. In particular if one wants to describe more neutron rich Zr isotopes a larger model space is required as the interaction between $(0g_{9/2})$ protons and $(2d_{3/2})$ and $(0g_{7/2})$ neutrons becomes increasingly important [6]. To our knowledge the present work is the first shell-model calculation of the Zr-isotopes which includes nuclei up to ^{98}Zr within a nontruncated $p:(1p_{1/2},0g_{9/2})n:(1d_{5/2},2s_{1/2},1d_{3/2},0g_{7/2},0h_{11/2})$ model space and with a fully realistic effective interaction.

We will in the present work perform a systematic shell-model study of the Zr isotopes from $N=50$ to $N=58$, and will in particular pay attention to the nuclei around the closure of the neutron $(1d_{5/2})$ and $(2s_{1/2})$ subshells, $^{96-98}$Zr. In several works we have performed thorough analyses of the effective two-body interaction. We have derived shell-model effective interactions based on meson exchange models for the free nucleon-nucleon interaction, using many-body perturbation theory as described below. The systems that have been studied are reaching from the oxygen region to the tin isotopes and the $N=82$ isotones, Refs. [10–13]. For the lighter systems, such as the sd- and pf-shell nuclei, we obtained markedly better results for nuclei with one kind of valence nucleons than for nuclei with both kinds. For the heavier systems we have so far restricted ourselves to nuclei with like valence nucleons, such as the Sn isotopes and the $N=82$ isotones. This way we have managed to keep the dimensionality of the eigenvalue problem within tractable limits. Further, we have seen the need for establishing confidence in the $T=1$ interaction before considering systems with both valence protons and neutrons, where the proton-neutron interaction may play a crucial role. In fact, the Zr isotopes represent a challenge on both these accounts.

Let us see in terms of a simplified model like the weak coupling scheme, in which the proton–neutron interaction is assumed to be weak, if one can gain insight into the qualitative properties of this interaction. In Fig. 2 we demonstrate the validity of this scheme by seeing how well it describes properties of ^{92,94,96}Zr. In column one the empirical spectrum of ^{90}Zr (dashed lines), which represents the proton degrees of freedom, is put on top of the ^{90}Sr spectrum (solid lines), which represents the neutron degrees of freedom. This would represent the ^{92}Zr spectrum in the weak coupling limit and should be compared with the empirical ^{92}Zr spectrum in column two. Similarly the weak coupling spectra ^{92}Sr+^{90}Zr and ^{94}Sr+^{90}Zr are compared with the empirical ^{94}Zr and ^{96}Zr spectra, respectively. Most states in ^{92}Zr and ^{94}Zr are well reproduced by the weak coupling scheme. The model does however collapse in ^{96}Zr, due to the presumed closure of the $1d_{5/2}$ subshell which does not have a counterpart in ^{94}Sr. The fact that the weak coupling scheme is fairly successful in describing ^{92}Zr and ^{94}Zr leads us to believe that

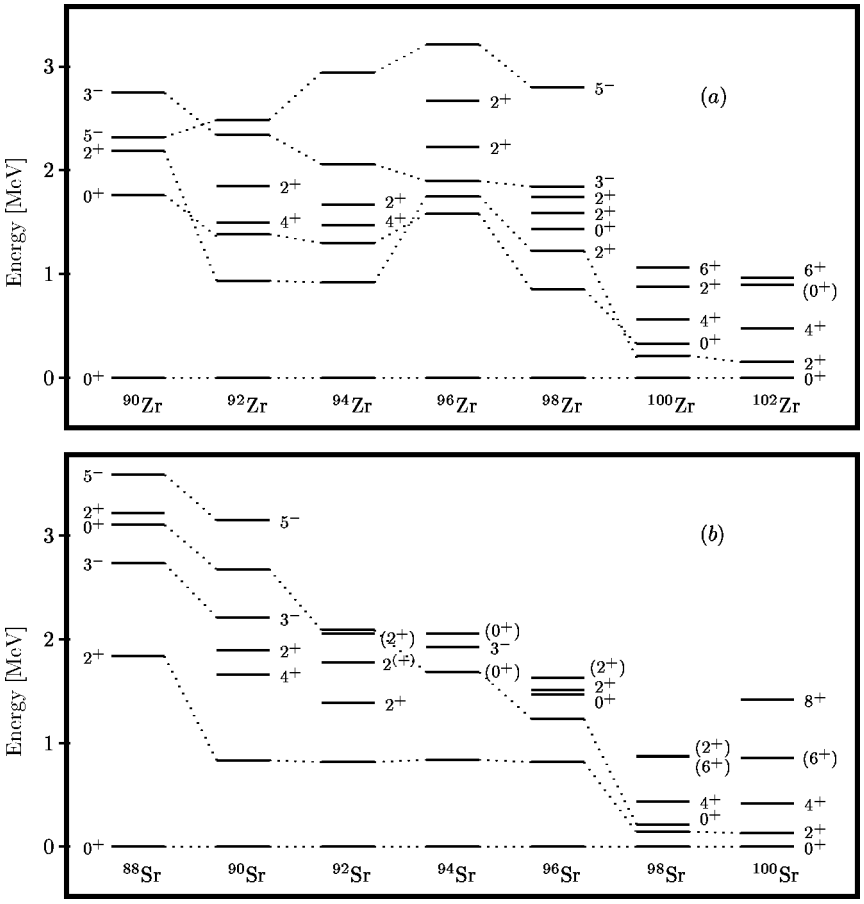

FIG. 1. Experimental low energy level schemes for the Zr (a) and Sr (b) isotopes from $N=50$ to $N=62$.

the proton-neutron part of the effective interaction is either rather weak or state-independent.

The paper is organized as follows. In Sec. II we give a summary of the calculation of the effective interaction and the shell model. Then the results are presented and discussed in Sec. III and conclusions are drawn in Sec. IV.

II. THEORETICAL FRAMEWORK

The aim of microscopic nuclear structure calculations is to derive various properties of finite nuclei from the underlying Hamiltonian describing the interaction between nucleons. When dealing with nuclei, such as the Zr isotopes with $A=90-100$, the full dimensionality of the many-body Schrödinger equation

$$H\Psi_i(1,\ldots,A)=E_i\Psi_1(1,\ldots,A), \tag{1}$$

becomes intractable and one has to seek viable approximations to Eq. (1). In Eq. (1), E_i and Ψ_i are the eigenvalues and eigenfunctions for a state i in the Hilbert space.

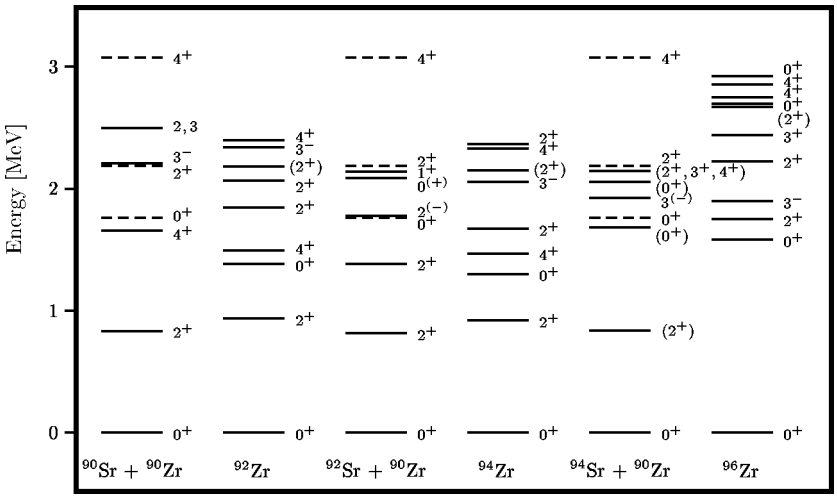

FIG. 2. Demonstration of the weak coupling scheme. The ^{90}Zr energy levels are represented by dashed lines. Experimental values are used for all levels energies.

One is normally only interested in solving Eq. (1) for certain low-lying states. It is then customary to divide the Hilbert space into a model space defined by the operator P and an excluded space defined by a projection operator $Q = 1 - P$

$$P = \sum_{i=1}^{d} |\psi_i\rangle\langle\psi_i|, \quad Q = \sum_{i=d+1}^{\infty} |\psi_i\rangle\langle\psi_i|, \tag{2}$$

with d being the size of the model space and such that $PQ = 0$. The assumption is that the low-lying states can be fairly well reproduced by configurations consisting of a few particles occupying physically selected orbitals, defining the model space. In the present work, the model space to be used both in the shell-model calculation and in the derivation of the effective interaction is given by the proton orbitals $1p_{1/2}$ and $0g_{9/2}$ and the neutron orbitals $2s_{1/2}$, $1d_{5/2}$, $1d_{3/2}$, $0g_{7/2}$, and $0h_{11/2}$.

Equation (1) can then be rewritten as a secular equation

$$PH_{\rm eff}P\Psi_i = P(H_0 + V_{\rm eff})P\Psi_i = E_i P\Psi_i, \tag{3}$$

where $H_{\rm eff}$ now is an effective Hamiltonian acting solely within the chosen model space. The term H_0 is the unperturbed Hamiltonian while the effective interaction is given by

$$V_{\rm eff} = \sum_{i=1}^{\infty} V_{\rm eff}^{(i)}, \tag{4}$$

with $V_{\rm eff}^{(1)}, V_{\rm eff}^{(2)}, V_{\rm eff}^{(3)}, \ldots$ being effective one-body, two-body, three-body interactions, etc. It is also customary in nuclear shell–model calculations to add the one-body effective interaction $V_{\rm eff}^{(1)}$ to the unperturbed part of the Hamiltonian so that

$$H_{\rm eff} = \tilde{H}_0 + V_{\rm eff}^{(2)} + V_{\rm eff}^{(3)} + \cdots, \tag{5}$$

where $\tilde{H}_0 = H_0 + V_{\rm eff}^{(1)}$. This allows us to replace the eigenvalues of $\tilde{H}_0$ by the empirical single-particle energies for the nucleon orbitals of our model space, or valence space. Thus, the remaining quantity to calculate is the two- or more-body effective interaction $\Sigma_{i=2}^{\infty} V_{\rm eff}^{(i)}$. In this work we will restrict our attention to the derivation of an effective two-body interaction

$$V_{\rm eff} = V_{\rm eff}^{(2)}, \tag{6}$$

using the many-body methods discussed in Ref. [14] and briefly reviewed below.

A. Effective interaction

Our procedure for obtaining an effective interaction for the Zr isotopes starts with a free nucleon-nucleon interaction $V^{(2)}$ which is appropriate for nuclear physics at low and intermediate energies. At present, there are several potentials available. The most recent versions of Machleidt and coworkers [15], the Nimjegen group [16], and the Argonne group [17] have all a χ^2 per datum close to 1. In this work we will thus choose to work with the charge-dependent version of the Bonn potential models, see Ref. [15]. The potential model of Ref. [15] is an extension of the one-boson-exchange models of the Bonn group [18], where mesons like π, ρ, η, δ, ω and the fictitious σ meson are included. In the charge-dependent version of Ref. [15], the first five mesons have the same set of parameters for all partial waves, whereas the parameters of the σ meson are allowed to vary.

The next step in our perturbative many-body scheme is to handle the fact that the strong repulsive core of the nucleon-nucleon potential V is unsuitable for perturbative approaches. This problem is overcome by introducing the reaction matrix G given by the solution of the Bethe-Goldstone equation

$$G = V + V\frac{Q}{\omega - QTQ}G, \tag{7}$$

where ω is the unperturbed energy of the interacting nucleons, and H_0 is the unperturbed Hamiltonian. The operator Q, commonly referred to as the Pauli operator, is a projection operator which prevents the interacting nucleons from scattering into states occupied by other nucleons. In this work we solve the Bethe-Goldstone equation for five starting energies ω, by way of the so-called double-partitioning scheme discussed in, e.g., Ref. [14]. The G matrix is the sum over all ladder type of diagrams. This sum is meant to renormalize the repulsive short-range part of the interaction. The physical interpretation is that the particles must interact with each other an infinite number of times in order to produce a finite interaction.

Finally, we briefly sketch how to calculate an effective two-body interaction for the chosen model space in terms of the G matrix. Since the G matrix represents just the summmation to all orders of ladder diagrams with particle-particle intermediate states, there are obviously other terms which need to be included in an effective interaction. Long-range effects represented by core-polarization terms are also needed. The first step then is to define the so-called $\hat{Q}$ box given by

$$P\hat{Q}P = PGP + P\left(G\frac{Q}{\omega - H_0}G + G\frac{Q}{\omega - H_0}G\frac{Q}{\omega - H_0}G + \cdots\right)P. \tag{8}$$

The $\hat{Q}$ box is made up of nonfolded diagrams which are irreducible and valence linked. A diagram is said to be irreducible if between each pair of vertices there is at least one hole state or a particle state outside the model space. In a valence-linked diagram the interactions are linked (via fermion lines) to at least one valence line. Note that a valence-linked diagram can be either connected (consisting of a single piece) or disconnected. In the final expansion including folded diagrams as well, the disconnected diagrams are found to cancel out [19]. This corresponds to the cancellation of unlinked diagrams of the Goldstone expansion [19]. These

TABLE I. Number of shell-model basis states in *m*-scheme SD representation.

n_p+n_n	Dimension	n_p+n_n	Dimension	n_p+n_n	Dimension
2 + 0	8	2 + 3	15 868	2 + 6	2 428 814
2 + 1	186	2 + 4	107 060	2 + 7	8 648 777
2 + 2	1 572	2 + 5	564 393	2 + 8	26 201 838

definitions are discussed in Refs. [14,19]. We can then obtain an effective interaction $H_{\rm eff}=\tilde{H}_0+V_{\rm eff}^{(2)}$ in terms of the $\hat{Q}$ box [14,19], with

$$V_{\rm eff}^{(2)}(n)=\hat{Q}+\sum_{m=1}^{\infty}\frac{1}{m!}\frac{d^m\hat{Q}}{d\omega^m}\{V_{\rm eff}^{(2)}(n-1)\}^m, \qquad (9)$$

where (n) and $(n-1)$ refer to the effective interaction after n and $n-1$ iterations. The zeroth iteration is represented by just the $\hat{Q}$ box. Observe also that the effective interaction $V_{\rm eff}^{(2)}(n)$ is evaluated at a given model space energy ω, as is the case for the G matrix as well. Here we choose $\omega=-20$ MeV. Moreover, although $\hat{Q}$ and its derivatives contain disconnected diagrams, such diagrams cancel exactly in each order [19], thus yielding a fully connected expansion in Eq. (9). Less than 10 iterations were needed in order to obtain a numerically stable result. All nonfolded diagrams through third order in the interaction G are included. For further details, see Ref. [14].

B. Shell model

The effective two-particle interaction can in turn be used in shell-model calculations. Our approach in solving the eigenvalue problem is the Lanczos algorithm, which is an iterative method that gives the solutions of the lowest eigenstates. The technique is described in detail in Refs. [20,21]. The shell-model code developed by us is designed for an *m*-scheme Slater determinant (SD) representation. Even with a rather restricted single-particle basis the size of the shell-model problem grows rapidly with increasing number of active valence particles. Table I shows how the number of configurations in an SD basis grows with the number of valence particles acting within the $(1p_{1/2}0g_{9/2})$ proton shell and the $(2s1d0g_{7/2}0h_{11/2})$ neutron shell relative to the ^{88}Sr core. Note that the ^{98}Zr system consists of more than 26 000 000 basis states. Only a few years ago shell-model calculations on such systems were not tractable. Even with today's fast computers and effective algorithms this kind of calculation is still rather time consuming.

TABLE II. Single-particle energies; all entries in MeV.

Single-proton energies			Single-neutron energies				
j_n	$1p_{1/2}$	$0g_{9/2}$	j_n	$1d_{5/2}$	$2s_{1/2}$	$1d_{3/2}$	$0g_{7/2}$	$0h_{11/2}$
$\varepsilon(j_n)$	0.00	0.90	$\varepsilon(j_n)$	0.00	1.26	2.23	2.63	3.50

The single-neutron energies are taken to be those deduced from ^{89}Sr in Refs. [22,23]. In the literature the single-proton energy splitting $\varepsilon(1p_{1/2})-\varepsilon(0g_{9/2})$ varies from 0.839 MeV to 1.0 MeV [7,8,24–26]. As the final results show little sensitivity to variations within this energy interval we let the $0g_{9/2}$ single-proton energy relative to $1p_{1/2}$ be 0.9 MeV. The single-particle energies used in this work are listed in Table II.

III. RESULTS AND DISCUSSIONS

In this section we present the calculations of the Zr isotopes. First, we analyze some systematics of the even Zr isotopes. The results are displayed in Figs. 3 and 4 (for some selected states) and in more detail in Tables IX, X, and XI. Then, we proceed with the discussion of the odd Zr isotopes, in Fig. 7 and Tables VII and VIII. A major aim is to investigate the effective interaction that has been derived for this mass region. Since the odd nuclei are generally more sensitive to the underlying assumptions made, this may give an even more severe test of the interaction and the foundations on which our model is based. At the end of this section we discuss problems concerning the binding energies. In order to study the effect of the proton degrees of freedom we have

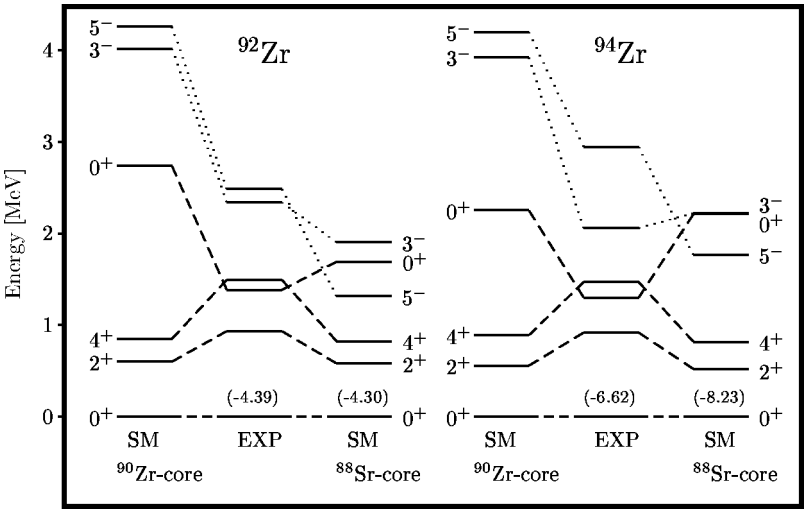

FIG. 3. Selected energy levels in ^{92}Zr and ^{94}Z. Numbers in parentheses are the binding energies of the valence nucleons outside a ^{88}Sr core.

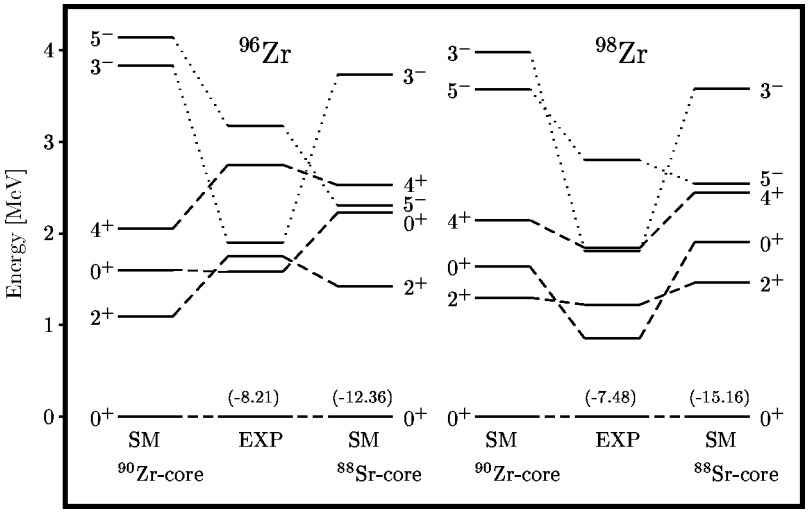

FIG. 4. Selected energy levels in ^{96}Zr and ^{98}Z. Numbers in parentheses are the binding energies of the valence nucleons outside a ^{88}Sr core.

also performed a more restricted calculation, considering only valence neutrons with respect to a ^{90}Zr core.

A. Even isotopes

The experimental spectra of the two nuclei, ^{92}Zr and ^{94}Zr, show very similar features. The shell-model calculation does also provide 0_1^+, 2_1^+, and 4_1^+ levels in ^{92}Zr and ^{94}Zr with quite similar features, although the three levels are too compressed compared to their experimental counterparts. Comparison of the results obtained with ^{90}Zr and ^{88}Sr cores indicates that these levels are little affected by proton excitations. In ^{96}Zr the calculated 0_1^+, 2_1^+, and 4_1^+ levels are still too compressed, though not as pronounced as in ^{92}Zr and ^{94}Zr, while in ^{98}Zr the calculated spectrum is more open than the experimental one.

The energy of the empirical 3_1^- level, Fig. 1(a), is monotonously reduced with increasing neutron number. In ^{92}Zr and ^{94}Zr the calculated 3_1^- level is obtained at about 2 MeV, while in ^{96}Zr and ^{98}Zr the 3_1^- level is obtained much too high at about 3.5 MeV. Due to the extension of the model space from a ^{90}Zr core to a ^{88}Sr core the 3_1^- level in ^{92}Zr and ^{94}Zr undergoes a considerable lowering, yielding results close to the experimental values. From the occupation numbers in Table III it is clear that the 3_1^- state undergoes a structural change from ^{94}Zr to ^{96}Zr. The $0g_{7/2}$ and $2s_{1/2}$ orbitals start to play a more important role. For comparison, the observed 3_1^- levels in Sr, Fig. 1(b), are all situated around 2 MeV. Their calculated counterparts are located too high, at about 3 MeV excitation energy. The structure of the 3_1^- level in Zr is totally different from the structure in Sr, Fig. 5. Let us look in detail into these states by comparing the 3_1^- levels in ^{92}Sr and ^{94}Zr. Both nuclei have four valence neutrons. In ^{92}Sr the dominant configuration is $[(1d_{5/2})^3 0h_{11/2}]_{J=3^-}$ whereas in ^{94}Zr the dominant configuration is $[(1p_{1/2}0g_{9/2})_{J_\pi=4^-,5^-}(1d_{5/2})^4_{J_\nu=2^+}]_{J=3^-}$. The difference can be ascribed to the single–particle energies. In Zr the 3_1^- state is created by exciting a proton into the $0g_{9/2}$ orbital instead of exciting a neutron into the $0h_{11/2}$ orbital. Because the $0h_{11/2}$ orbital is located very high in the single-particle spectrum it is more favorable to excite a proton rather than a neutron.

The situation for the 5_1^- level is more stable throughout the whole sequence of Zr isotopes, with empirical values between 2.5 and 3.0 MeV. The ^{90}Zr-core calculations provide level energies that are 1.0–1.5 MeV too high, while the ^{88}Sr-core calculations give energies too low by about 1 MeV. This state consists predominantly of configurations with a proton excited into the $0g_{9/2}$ orbital and the neutrons remaining in the lowest possible single-particle orbitals.

As pointed out in the Introduction, there are strong variations in the structure from one nucleus to another, reflected in for instance the 0^+-2^+ spacing. Qualitatively we reproduce the variation in the 0^+-2^+ spacing quite well, as

TABLE III. Occupation numbers of the 2_1^+, 4_1^+, 3_1^-, and 5_1^- states in $^{92-98}$Zr.

	J_i^π	$0g_{9/2}$	$1p_{1/2}$	$0h_{11/2}$	$0g_{7/2}$	$1d_{5/2}$	$1d_{3/2}$	$2s_{1/2}$
^{92}Zr:								
	2_1^+	0.27	1.73	0.02	0.01	1.92	0.02	0.04
	4_1^+	0.24	1.76	0.01	0.01	1.96	0.02	0.01
	3_1^-	0.98	1.02	0.05	0.03	1.67	0.08	0.18
	5_1^-	1.00	1.00	0.05	0.04	1.79	0.07	0.05
^{94}Zr:								
	2_1^+	0.15	1.85	0.06	0.01	3.79	0.06	0.08
	4_1^+	0.13	1.87	0.05	0.01	3.87	0.05	0.02
	3_1^-	0.99	1.01	0.08	0.05	3.52	0.15	0.20
	5_1^-	1.00	1.00	0.11	0.08	3.48	0.18	0.14
^{96}Zr:								
	2_1^+	0.12	1.88	0.09	0.03	4.75	0.13	1.01
	4_1^+	0.14	1.86	0.09	0.04	4.78	1.02	0.08
	3_1^-	0.97	1.03	0.14	0.76	4.52	0.20	0.39
	5_1^-	0.98	1.02	0.16	0.09	5.21	0.25	0.29
^{98}Zr:								
	2_1^+	0.10	1.90	0.12	0.05	5.76	1.10	0.97
	4_1^+	0.18	1.82	0.15	0.98	5.66	0.21	1.01
	3_1^-	0.99	1.01	0.15	0.55	5.55	1.13	0.63
	5_1^-	0.91	1.09	0.28	0.21	5.58	0.36	1.57

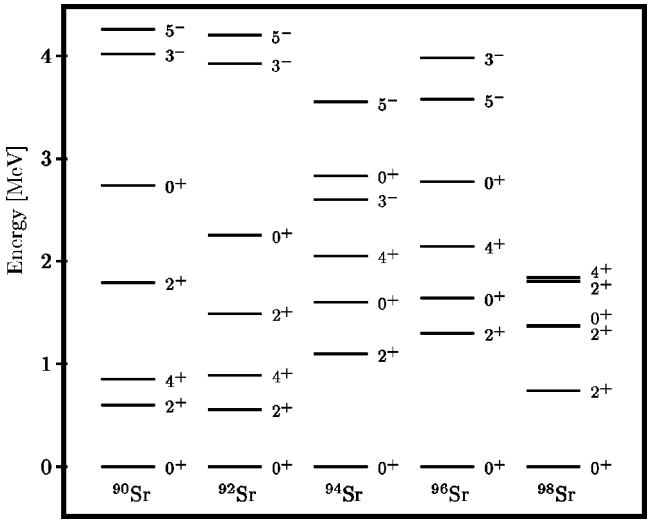

FIG. 5. Calculated energy levels for the Sr isotopes from $N=52$ to $N=60$. The experimental levels are shown in Fig. 1(b).

shown in Fig. 6, although in $^{90-96}$Zr the gap is 200–400 keV less than the experimental spacing.

In spite of clear differences in the experimental Zr and Sr spectra, the shell-model calculation provides rather similar results. The calculated Zr spectra are in far better agreement with experimental data than the calculated Sr spectra, which may indicate that the core is in a different condition in the two systems. In Sr the core seems to be relatively soft, whereas in Zr the two additional protons tend to stabilize the core.

1. Proton configurations

The proton degrees of freedom are crucial in order to describe certain energy levels. For example, the first excited 0_2^+ state in ^{92}Zr has strong components of proton excitations. From the occupation numbers in Table IV we see that the character of 0_1^+ state is totally different from the 0_2^+ state. The proton parts of their wave functions are almost orthogonal to each others. In the ground state the protons are most likely to be found in the $1p_{1/2}$ orbital, while for the excited 0^+ state it is more probable to find the protons in the $0g_{9/2}$ orbital. However, in ^{96}Zr the two shell-model 0^+ states have

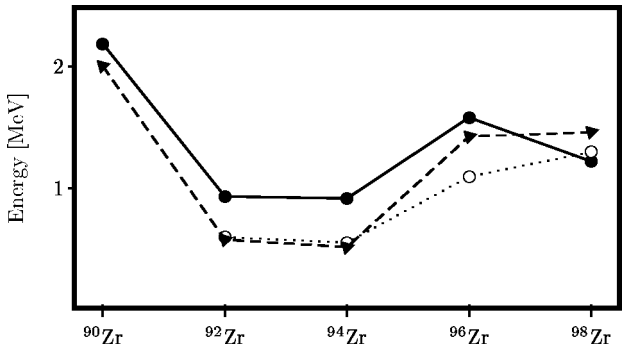

FIG. 6. The 2_1^+ excitation energy, experimental (solid) and calculated, complete (dashed) and without pp and pn interaction (dotted), respectively.

TABLE IV. Occupation numbers of the three lowest-lying 0^+ states in $^{92-98}$Zr.

	J_i^π	$0g_{9/2}$	$1p_{1/2}$	$0h_{11/2}$	$0g_{7/2}$	$1d_{5/2}$	$1d_{3/2}$	$2s_{1/2}$
^{92}Zr:								
	0_1^+	0.33	1.67	0.06	0.03	1.81	0.07	0.03
	0_2^+	1.70	0.30	0.05	0.15	1.61	0.11	0.08
	0_3^+	1.30	0.70	0.07	0.14	0.63	0.06	1.11
^{94}Zr:								
	0_1^+	0.17	1.83	0.10	0.04	3.69	0.11	0.06
	0_2^+	1.78	0.23	0.13	0.49	2.75	0.31	0.33
	0_3^+	0.42	1.58	0.08	0.06	2.09	0.12	1.65
^{96}Zr:								
	0_1^+	0.09	1.91	0.12	0.03	5.66	0.12	0.07
	0_2^+	0.22	1.78	0.13	0.09	3.88	0.15	1.76
	0_3^+	1.76	0.24	0.19	0.96	3.86	0.47	0.52
^{98}Zr:								
	0_1^+	0.09	1.91	0.15	0.06	5.76	0.17	1.87
	0_2^+	0.44	1.56	0.27	0.72	5.50	1.26	0.26
	0_3^+	1.41	0.59	0.19	1.46	4.79	0.98	0.58

nearly the same proton structure, almost pure $(1p_{1/2}^2)_\pi$ configuration. The 0^+ levels in ^{98}Zr show similar structure as in ^{96}Zr, but the 0_2^+ state has slightly stronger $0g_{9/2}$ mixing than in ^{96}Zr. The third 0^+ state in both ^{96}Zr and ^{98}Zr have $(0g_{9/2})$ as the predominant proton configuration. The change in the proton configuration with increasing neutron number was observed in pick-up experiments by Saha *et al.* [27].

2. Subshell closure

Clear signs of subshell closure are seen in ^{96}Zr and also in ^{98}Zr, due to filling of the $1d_{5/2}$ and the $2s_{1/2}$ orbitals, respectively. From ^{94}Zr to ^{96}Zr the gap between the ground state and the 2_1^+ state is doubled. The experimental $0_1^+ \rightarrow 2_1^+$ gap increases, from 0.919 MeV in ^{94}Zr to 1.751 MeV in ^{96}Zr, and the calculated gap is also more than doubled, from 0.520 MeV to 1.426 MeV. In ^{98}Zr the calculated spacing is larger than the experimental one. The experimental 0^+-2^+ spacing is 1.223 MeV, and the corresponding calculated spacing 1.463 MeV. The ^{96}Zr ground state $1d_{5/2}$ occupation number is 5.66, and in ^{98}Zr the $1d_{5/2}$ and $2s_{1/2}$ occupation numbers are 5.76 and 1.87, respectively.

The total impression of the ^{98}Zr shell-model results displayed in Fig. 4 is disappointing. Only the 2_1^+ level is reasonably reproduced. As an alternative to the extremely time and space consuming calculation presented in Fig. 4, we may close the $1d_{5/2}$ orbital and perform a ^{94}Sr-core shell-model calculation of the system. The results, shown in Table XI, are much improved.

3. E2 transition rates

Experimental and calculated $E2$ transition rates are tabulated in Table V. In order to bring the theoretical results into agreement with the measured $2_1^+ \rightarrow 0_1^+$ transition rates we have employed effective charges of $1.8e$ and $1.5e$ for the protons and neutrons, respectively. These values are consis-

TABLE V. $E2$ transition rates. Numbers in parentheses indicate uncertainties in the last digit of the quoted experimental values. The proton and neutron effective charges are set equal to zero in columns 5 and 6, respectively. All entries in Weisskopf units (W.u.).

	Transition	Expt.	Calc.		
	$B(E2;J_i^\pi \to J_f^\pi)$		$e_p^{\rm eff}=1.8,\ e_n^{\rm eff}=1.5$	$e_p^{\rm eff}=0.0$	$e_n^{\rm eff}=0.0$
^{90}Zr	$B(E2;2_1^+ \to 0_1^+)$	5.37 (20)	1.88		
	$B(E2;2_1^+ \to 0_2^+)$	5.2 (10)	6.21		
	$B(E2;8_1^+ \to 6_1^+)$	2.40 (16)	2.57		
^{92}Zr	$B(E2;2_1^+ \to 0_1^+)$	6.4 (6)	2.97	2.54	0.02
	$B(E2;0_2^+ \to 2_1^+)$	14.3 (5)	0.30	0.11	0.77
	$B(E2;4_1^+ \to 2_1^+)$	4.04 (12)	0.40	0.30	0.01
	$B(E2;6_1^+ \to 4_1^+)$	>0.00098	0.24	0.002	0.20
^{94}Zr	$B(E2;2_1^+ \to 0_1^+)$	4.4 (5)	3.69	3.56	0.001
	$B(E2;0_2^+ \to 2_1^+)$	9.3 (4)	0.01	0.05	0.11
	$B(E2;4_1^+ \to 2_1^+)$	0.876 (23)	1.26	1.22	0.0004
^{96}Zr	$B(E2;2_1^+ \to 0_1^+)$	4 (3)	0.05	0.03	0.002
	$B(E2;2_2^+ \to 0_1^+)$	>0.020	0.13	0.10	0.002
	$B(E2;2_2^+ \to 0_2^+)$	>2.7	1.17	1.03	0.005
^{98}Zr	$B(E2;2_1^+ \to 0_1^+)$	>0.24	0.02	0.01	0.0005
	$B(E2;2_1^+ \to 0_2^+)$	>0.04	0.64	0.48	0.01
	$B(E2;0_3^+ \to 2_1^+)$	51 (5)	≈ 0.00	0.02	0.02

tent with the effective charges obtained in Refs. [6,26,28], however a bit overestimated compared to the fitting to data on ^{92}Mo and ^{91}Zr done by Halse in Ref. [7]. To be mentioned, the calculation of effective charges based on perturbative many-body methods [29] gives much smaller values, $1.1e$ and in the range $0.5e-0.7e$ for the proton and neutron effective charge, respectively.

We adopt Halse's effective value of the oscillator parameter $b=2.25$ fm. The value was choosen by reference to measurements for the radii of the single–particle orbitals in ^{89}Sr and of the charge distributions in $^{92-96}$Mo, Refs. [22] and [30].

With effective charges and the oscillator parameter as described above, the transition rates between yrast states are fairly well reproduced. In the former discussion we have focused on the 0_2^+ state, in particlular its proton structure. In ^{92}Zr and ^{94}Zr we totally fail in reproducing the transition rates involving the 0_2^+ state. The experimental transition rates between 0_2^+ and 2_1^+ in ^{92}Zr and ^{94}Zr are relatively strong, 14.3(5) and 9.3(4) W.u., respectively, whereas the calculated transition rates are two to three orders of magnitude smaller. Similarly, in ^{98}Zr there is an experimental transition rate between 0_3^+ and 2_1^+ with strength 51(5) W.u. The corresponding calculated transition rate is negligible. In fact, the occupation numbers in Table IV show that the 0_3^+ state in ^{98}Zr has similar proton structure to the 0_2^+ state in ^{92}Zr and ^{94}Zr. Leaving out the neutron contributions, as done in column 6 of Table V, by setting the effective neutron charge equal to zero, we observe that the proton part of the wave function contributes more to the transitions involving the excited 0^+ states than what it does to the other transition rates. The contribution is however far from sufficient and there is a cancellation effect between the proton and neutron contributions. Contributions to the transition rates between yrast states do on the other hand mainly stem from the neutron degrees of freedom. In conclusion, it seems that the 0_2^+ states in ^{92}Zr and ^{94}Zr and the 0_3^+ state in ^{98}Zr contain strong collective components not reproduced by the present shell model calculation.

B. Odd isotopes

It is somehow surprising to notice that the shell model gives a much better description of the odd than of the even Zr isotopes. The reproduction of the low-lying positive parity states are overall satisfactory. On the other hand the shell model has some problems in describing the negative parity states. Several of the negative parity states in ^{91,93}Zr are calculated up to 1 MeV too low. Only a few negative parity states are known in ^{95,97}Zr. Thus a detailed comparison is difficult, but the $11/2_1^-$ state is reproduced in nice agreement with experiment.

We will make a detailed study of ^{93}Zr. This nucleus is not too simple and not too complex (two protons and three neutrons outside the closed core), and useful information can therefore be extracted from a few central and relatively simple configurations.

The shell-model calculation provides three states below 600 keV, $5/2_1^+$, $3/2_1^+$, and $9/2_1^+$. From experiments, only two states are known, $5/2_1^+$ and $3/2_1^+$. There are however theoretical arguments supporting a low-lying $9/2_1^+$ state. The configuration that requires the least energy has all particles in the lowest possible single-particle orbital. In the case of ^{93}Zr the two protons occupy the $1p_{1/2}$ single-particle orbital, and couple to $J=0$. The three neutrons occupy the $1d_{5/2}$ orbital $(1d_{5/2}^3)_\nu$. The three neutrons can then couple to $J^\pi=3/2^+$, $5/2^+$, or $9/2^+$. Such states will be located well below 1 MeV. The lowest experimental $9/2^+$ candidate observed up to now is seen at 1.46 MeV.

TABLE VI. Occupation numbers in ^{97}Zr.

	J_i^π	$0g_{9/2}$	$1p_{1/2}$	$0h_{11/2}$	$0g_{7/2}$	$1d_{5/2}$	$1d_{3/2}$	$2s_{1/2}$
^{97}Zr:	$1/2_1^+$	0.09	1.91	0.11	0.03	5.73	0.15	0.99
	$3/2_1^+$	0.10	1.90	0.11	0.04	5.72	1.04	0.08
	$5/2_1^+$	0.11	1.89	0.12	0.05	4.83	0.14	1.87
	$7/2_1^+$	0.26	1.74	0.15	1.00	5.51	0.17	0.17
	$5/2_2^+$	0.15	1.85	0.10	0.05	4.77	1.06	1.04
	$7/2_2^+$	0.14	1.86	0.11	0.05	4.82	1.04	0.99
	$3/2_2^+$	0.18	1.82	0.11	0.06	4.77	1.08	0.98
	$11/2_1$	0.88	1.12	0.26	0.07	5.83	0.27	0.88

As many as four $1/2^+$ states are observed within a small energy interval of 250 keV in the region from 0.95 MeV to 1.22 MeV. This observation has no shell-model counterpart. Our calculation provides only one $1/2^+$ level at 1.40 MeV.

We already pointed out that our model has difficulty in describing the negative parity states. Consider for example the structure of the $11/2_1^-$ state in ^{93}Zr, which comes 500 keV lower than the experimental position. Odd parity states are constructed by configurations with an odd number of particles in negative parity states. Within our model, protons can occupy the $1p_{1/2}$ orbital and neutrons can occupy the $0h_{11/2}$ orbital to produce negative parity states. Both the first and second excited $11/2^-$ states in ^{93}Zr are predominantly based on the proton configuration $(1p_{1/2}0g_{9/2})_\pi$. The same is true for the $11/2_1^-$ state in the other Zr isotopes.

Finally, we examine ^{97}Zr. As we would expect for a system caught in between two ''magic'' nuclei we recognize pronounced single-particle structure. From the occupation numbers, listed in Table VI, we see that both the ground state, $1/2_1^+$, and the next level, $3/2_1^+$, are pure one-quasiparticle states built on a full $1d_{5/2}$ orbital, i.e., ^{96}Zr core. Also the $7/2_1^+$ state is a one-quasiparticle state with the $1d_{5/2}$ orbital nearly closed, though its calculated position is about 0.7 MeV too high. This means that a somewhat lower single-particle energy $\varepsilon_{0g_{9/2}}$ might be more appropriate for our effective interaction. The $5/2_1^+$ state can be regarded as a $1d_{5/2}$-hole state relative to the ^{98}Zr core. All in all the yrast states apart from $7/2^+$ are very well reproduced. In the other, nonyrast states, the ^{96}Zr core breaks up and two neutrons are distributed equally among the $2s_{1/2}$ and $1d_{3/2}$ orbitals. (See Fig. 7 and Tables VII and VIII.)

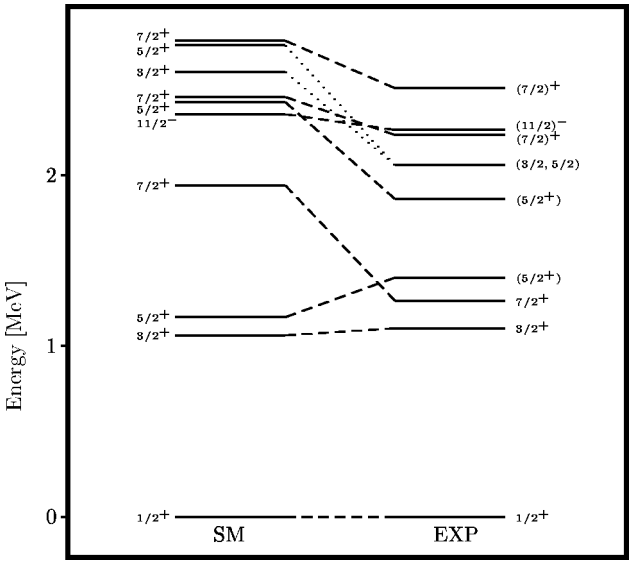

FIG. 7. Theoretical and experimental spectra of ^{97}Zr.

C. Binding energies

The binding energies calculated by the formula

$$\begin{aligned} \mathrm{BE}(^{90+n}\mathrm{Zr}) = \mathrm{BE}(^{90+n}\mathrm{Zr}) - \mathrm{BE}(^{88}\mathrm{Sr}) \\ - n(\mathrm{BE}(^{89}\mathrm{Sr}) - \mathrm{BE}(^{88}\mathrm{Sr})) \\ - 2(\mathrm{BE}(^{89}\mathrm{Y}) - \mathrm{BE}(^{88}\mathrm{Sr})) \end{aligned} \quad (10)$$

TABLE VII. Theoretical and experimental energy levels in ^{91}Zr and ^{93}Zr. Energies are given in MeV.

^{91}Zr				^{93}Zr			
J^π	SM	J^π	Expt.	J^π	SM	J^π	Expt.
$5/2^+$	0.0	$5/2^+$	0.0	$5/2^+$	0.0	$5/2^+$	0.0
$1/2^+$	1.477	$1/2^+$	1.205	$3/2^+$	0.182	$3/2^+$	0.269
$5/2^+$	1.717	$5/2^+$	1.466	$9/2^+$	0.568	$1/2^+$	0.947
$7/2^+$	2.015	$7/2^+$	1.882	$1/2^+$	1.307	$1/2^+$	1.018
$9/2^+$	2.094	$3/2^+$	2.042	$7/2^+$	1.686	$1/2^+$	1.169
$3/2^+$	2.361	$(9/2)^+$	2.131	$3/2^+$	1.755	$1/2^+$	1.222
$7/2^+$	2.383	$7/2^+$	2.201	$5/2^+$	1.895	$3/2^+,5/2^+$	1.425
$13/2^+$	2.403	(5/2,7/2)	2.367	$5/2^+$	2.114	$(1/2^+,3/2,5/2^+)$	1.450
$5/2^+$	2.405	$3/2^+,5/2^+$	2.535	$3/2^+$	2.208	$9/2^+,7/2^+$	1.463
$11/2^+$	2.444	$1/2^+$	2.558	$7/2^+$	2.211	$(1/2^+,3/2,5/2^+)$	1.470
$5/2^-$	1.063	$(11/2)^-$	2.170	$13/2^-$	1.417	$(9/2^-,11/2^-)$	2.025
$15/2^-$	1.173	$(5/2)^-$	2.190	$9/2^-$	1.445	$(9/2^-,11/2^-)$	2.363
$13/2^-$	1.423	$(13/2)^-$	2.260	$11/2^-$	1.507	$(9/2^-,11/2^-)$	2.662
$11/2^-$	1.430	$(15/2)^-$	2.288				
$7/2^-$	1.520	$(11/2)^-$	2.321				

TABLE VIII. Theoretical and experimental energy levels in ^{95}Zr and ^{97}Zr. Energies are given in MeV.

^{95}Zr				^{97}Zr			
J^π	SM	J^π	Expt.	J^π	SM	J^π	Expt.
$5/2^+$	0.0	$5/2^+$	0.0	$1/2^+$	0.0	$1/2^+$	0.0
$1/2^+$	1.021	$1/2^+$	0.954	$3/2^+$	1.062	$3/2^+$	1.103
$3/2^+$	1.285	$3/2^+,5/2^+$	1.14	$5/2^+$	1.168	$7/2^+$	1.264
$7/2^+$	1.482	$3/2^+,5/2^+$	1.324	$7/2^+$	1.940	$(5/2^+)$	1.400
$5/2^+$	1.613	$7/2^+,9/2^+$	1.618	$5/2^+$	2.427	$(5/2^+)$	1.859
$9/2^+$	1.857	$(3/2)^+$	1.618	$7/2^+$	2.457	$(5/2^+)$	1.997
$3/2^+$	2.051	$(5/2)^+$	1.722	$3/2^+$	2.604	(3/2,5/2)	2.058
$7/2^+$	2.306	$1/2^{(+)},3/2,5/2^+$	1.904	$9/2^+$	2.644	$(7/2)^+$	2.234
$1/2^+$	2.414	$1/2^{(+)},3/2,5/2^+$	1.940	$5/2^+$	2.759	$(7/2)^+$	2.508
$5/2^+$	2.490	$5/2^{(+)}$	1.956	$7/2^+$	2.786	$(7/2)^+$	3.161
$13/2^-$	1.919	$9/2^-,11/2^-$	2.025	$11/2^-$	2.356	$(7/2^-)$	1.807
$11/2^-$	2.039	$1/2^-,3/2^-$	2.816	$9/2^-$	2.492	$(11/2^-)$	2.264

are plotted in Fig. 8. In Eq. (10) n is the number of valence neutrons. The experimental binding energies show a parabola structure with a minimum at ^{96}Zr, whereas the calculated binding energies increase linearly down to ^{98}Zr. With increasing neutron number the systems become far too strongly bound. This phenomenon of overbinding of nuclear systems when effective interactions from meson theory are used has been much discussed in the literature, for example in Ref. [31]. The solutions to the problem has been that such matrix elements must be modified in order to reproduce the binding energies correctly. The so-called centroid matrix elements should be corrected in order to reproduce experiment. However, there is no well-defined recipe for doing this.

The curve labeled ''no pn-int'' in Fig. 8 shows the binding energies with the proton-neutron interaction switched off. Now, the systems are too weakly bound, which tells us that the proton-neutron part of the interaction contributes strongly to the overbinding. We have made the pn interaction less attractive by adding an overall constant to the diagonal matrix elements. This will not affect the excitation energies relative to the ground state. The constant is chosen such as to fit the experimental binding energy of ^{90}Y. Thus, a constant 0.3 MeV added to the original diagonal proton-neutron matrix elements, $V^{\rm mod}_{\rm abab}({\rm pn}) = V^{\rm eff}_{\rm abab}({\rm pn}) + 0.3$ MeV, gives binding energies as shown in Fig. 8, labeled ''modified pn-int.'' The fit to the experimental values are much improved, although there is a linear rather than parabolic dependence on the particle number.

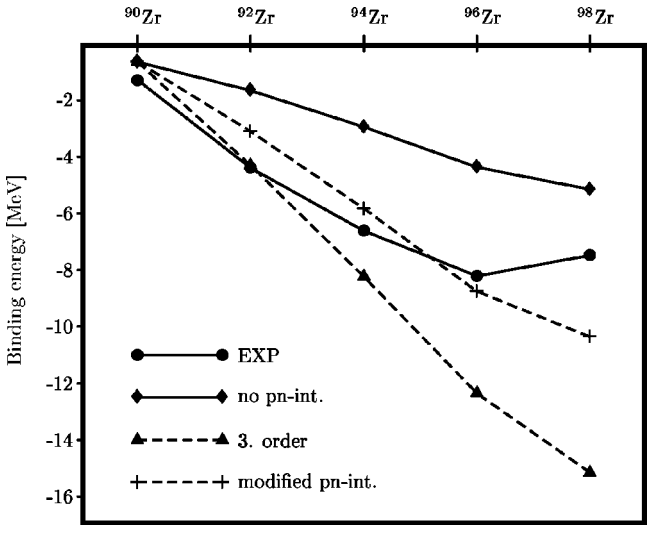

FIG. 8. Relative binding energies of ^{90}Zr-^{98}Zr. The curves show the experimental and theoretical binding energy curves, the full shell-model calculation, calculations without the pn interaction, and calculations with modified pn interaction, respectively.

IV. CONCLUSIONS

In this work we have performed a full $(1p_{1/2}0g_{9/2})$ proton and $(2s1d0g_{7/2}0h_{11/2})$ neutron shell-model calculation of the zirconium isotopes ranging from $N=52$ to $N=60$. For the first time we present results from calculations with a proton-neutron effective interaction in such heavy nuclei.

We have succeeded in obtaining a qualitative reproduction of important properties, although there are also shortcomings. The odd isotopes are very well described by our shell model, in fact better than the calculated even isotopes.

TABLE IX. Low-lying states in ^{90}Zr and ^{92}Zr. Energies are given in MeV.

^{90}Zr			^{92}Zr			
J^π	^{88}Sr core	Expt.	J^π	^{90}Zr core	^{88}Sr core	Expt.
0_2^+	1.706	1.761	0_2^+	2.738	1.693	1.383
2_1^+	2.003	2.186	2_1^+	0.601	0.581	0.935
2_2^+		3.309	2_2^+	1.792	1.921	1.847
			2_3^+	3.093	2.167	2.067
3_1^-		2.748	3_1^-	4.018	1.904	2.340
4_1^+	2.235	3.077	4_1^+	0.850	0.823	1.496
4_1^-	1.693	2.739	4_2^+	2.677	2.379	2.398
5_1^-		2.319	5_1^-	4.261	1.316	2.486
6_1^+	2.317	3.448	6_1^+	3.206	2.596	

TABLE X. Low-lying states in ^{94}Zr and ^{96}Zr. Energies are given in MeV.

	^{94}Zr				^{96}Zr		
J^π	^{90}Zr core	^{88}Sr core	Expt.	J^π	^{90}Zr core	^{88}Sr core	Expt.
0_2^+	2.254	2.213	1.300	0_2^+	1.602	2.228	1.582
2_1^+	0.557	0.520	0.919	2_1^+	1.097	1.426	1.751
2_2^+	1.490	1.764	1.671	2_2^+	2.105	2.661	2.226
2_3^+	1.930	2.228	2.151	2_3^+	2.211	2.768	2.669
3_1^-	3.923	2.223	2.058	3_1^-	3.833	3.732	1.897
4_1^+	0.889	0.817	1.470	4_1^+	2.054	2.528	2.750
4_2^+	1.898	2.162	2.330	4_2^+	2.230	2.869	2.857
5_1^-	4.200	2.673	2.945	5_1^-	4.141	2.306	3.120

Both for the odd and the even nuclei we have difficulties in reproducing the negative parity states well.

For comparison we have presented shell-model results for the neighboring strontium isotopes. The qualitative features are much better reproduced in Zr than in Sr. For example, the shell model fails in reproducing the very stable 0^+-2^+ spacing in Sr. Differently from Zr, there is no sign of $N=56$ and $N=58$ subshell closures in Sr. The quality of the closed-shell core (^{88}Sr) may in fact be different for the two sets of isotopes. It is likely that the additional protons in Zr give a more balanced system and serve to stabilize the core. In Sr the core seems to be softer and more unstable.

The empirical Zr spectra can to a certain extent be interpreted in a weak coupling scheme. The isotopes ^{92}Zr and ^{94}Zr are well described in terms of this model, which in turn indicates that the proton-neutron interaction should not be too strong. The simple weak coupling picture collapses however in ^{96}Zr.

In order to obtain results for ^{98}Zr, we performed calculations that are extremely heavy and time consuming. All the efforts gave final results that were far off, and in fact a much simpler calculation based on a ^{94}Sr core provided results in better agreement with the experimental data.

The occupation numbers give a hint that the $0g_{7/2}$ and the $0h_{11/2}$ neutron orbitals are of minor importance. The major properties are in fact fairly well described within a reduced basis $(1p_{1/2},0g_{9/2})_\pi(2s_{1/2},1d_{5/2},1d_{3/2})_\nu$.

TABLE XI. Low-lying states in ^{98}Zr. Energies are given in MeV.

	^{98}Zr			
J^π	^{90}Zr core	^{88}Sr core	^{94}Sr core	Expt.
0_2^+	1.641	1.904	0.529	0.854
0_3^+	2.773	2.471	1.969	1.859
2_1^+	1.300	1.463	1.152	1.223
2_2^+	2.207	2.619	1.773	1.591
2_3^+	2.442		2.149	1.744
3_1^-	3.983	3.579	2.597	1.806
4_1^+	2.147	2.449	1.574	1.843
4_2^+	2.048	2.650	1.918	2.330
5_1^-	3.576	3.478	1.318	2.800

In order to further test the wave functions we calculated $E2$ transition rates in the even Zr isotopes. Transitions between yrast states are fairly well reproduced, whereas transitions involving certain excited 0^+ states are calculated far too small, indicating that these states contain strong components not accounted for by the present shell model.

As in other mass regions we fail in reproducing bulk properties such as the binding energies. With increasing number of valence nucleons the systems become far too strongly bound. We have demonstrated that this problem can be cured by simple adjustments of some selected matrix elements.

ACKNOWLEDGMENTS

The calculations have been carried out at the IBM cluster at the University of Oslo. Support for this from the Research Council of Norway (NFR) is acknowledged.

APPENDIX: TABLES

The low-lying experimental and calculated energy levels in $^{90-98}$Zr are listed in Tables IX, X and XI.

[1] F. Schussler, J. A. Pinston, E. Monnand, A. Moussa, G. Jung, E. Koglin, B. Pfeiffer, R. V. F. Janssens, and J. van Klinken, Nucl. Phys. **A339**, 415 (1980).
[2] K. Becker, G. Jung, K.-H. Kobras, H. Wollnik, and B. Pfeiffer, Z. Phys. A **319**, 193 (1984).
[3] H. Mach, M. Moszyński, R. L. Gill, J. A. Winger, John C. Hill, G. Molńar, and K. Sistemich, Phys. Lett. B **230**, 21 (1989).
[4] G. Lhersonneau *et al.*, Phys. Rev. C **56**, 2445 (1997).
[5] G. Lhersonneau *et al.*, Phys. Rev. C **49**, 1379 (1994); G. Lhersonneau *et al.*, *ibid.* **54**, 1117 (1996).
[6] D. H. Gloeckner, Phys. Lett. **42B**, 381 (1972); D. H. Gloeckner, Nucl. Phys. **A253**, 301 (1975).
[7] P. Halse, J. Phys. G **19**, 1859 (1993).
[8] S. S. Ipson, K. C. McLean, W. Booth, J. G. B. Haigh, and R. N. Glover, Nucl. Phys. **A253**, 189 (1975).
[9] N. Auerbach and I. Talmi, Nucl. Phys. **64**, 458 (1965).
[10] T. Engeland, M. Hjorth-Jensen, A. Holt, and E. Osnes, Phys. Rev. C **48**, 535 (1993).
[11] A. Holt, T. Engeland, M. Hjorth-Jensen, E. Osnes, and J. Suhonen, Nucl. Phys. **A618**, 107 (1997).
[12] J. Suhonen, J. Toivanen, A. Holt, T. Engeland, M. Hjorth-Jensen, and E. Osnes, Nucl. Phys. **A628**, 41 (1998).
[13] A. Holt, T. Engeland, M. Hjorth-Jensen, and E. Osnes, Nucl. Phys. **A634**, 41 (1998).
[14] M. Hjorth-Jensen, T. T. S. Kuo, and E. Osnes, Phys. Rep. **261**, 125 (1995).
[15] R. Machleidt, F. Sammarruca, and Y. Song, Phys. Rev. C **53**, 1483 (1996).
[16] V. G. J. Stoks, R. A. M. Klomp, C. P. F. Terheggen, and J. J. de Swart, Phys. Rev. C **48**, 792 (1993).

[17] R. B. Wiringa, V. G. J. Stoks, and R. Schiavilla, Phys. Rev. C **51**, 38 (1995).
[18] R. Machleidt, Adv. Nucl. Phys. **19**, 189 (1989).
[19] T. T. S. Kuo and E. Osnes, *Folded-Diagram Theory of the Effective Interaction in Atomic Nuclei*, Lecture Notes in Physics Vol. 364 (Springer, Berlin, 1990).
[20] R. R. Whitehead, A. Watt, B. J. Cole, and I. Morrison, Adv. Nucl. Phys. **9**, 123 (1977).
[21] T. Engeland, M. Hjorth-Jensen, A. Holt, and E. Osnes, Phys. Scr. **T56**, 58 (1995).
[22] A. Saganek, V. Meyer, S. Mirowski, M. Oteski, M. Siemeáski, E. Wesolowski, and Z. Wilhelmi, J. Phys. G **10**, 549 (1984).
[23] T. P. Cleary, Nucl. Phys. **A301**, 317 (1978).
[24] S. Ramavataram, B. Goulard, and J. Bergeron, Nucl. Phys. **A207**, 140 (1973).
[25] P. Hoffmann-Pinther and J. L. Adams, Nucl. Phys. **A229**, 365 (1974).
[26] D. S. Chuu, M. M. King Yen, Y. Shan, and T. Hsien, Nucl. Phys. **A321**, 415 (1979).
[27] A. Saha, G. D. Jones, L. W. Put, and R. H. Siemssen, Phys. Lett. **82B**, 208 (1979).
[28] B. A. Brown, P. M. S. Lesser, and D. B. Fossan, Phys. Rev. C **13**, 1900 (1976).
[29] M. Hjorth-Jensen (unpublished).
[30] L. Schellenberg, B. Robert-Tissot, K. Kaeser, L. A. Schaller, H. Schneuwly, G. Fricke, S. Gluckert, G. Mallot, and E. B. Shere, Nucl. Phys. **A333**, 333 (1980).
[31] A. P. Zuker, Nucl. Phys. **A576**, 65 (1994); G. Martinez-Pinedo, A. P. Zuker, A. Poves, and E. Caurier, Phys. Rev. C **55**, 187 (1997).